THE SPLASHBACK RADIUS OF PLANCK-SZ CLUSTERS

Dominik Zürcher [1, 2, 4] Surhud More [3, 1],
[1]Kavli Institute for the Physics and Mathematics of the Universe (Kavli IPMU, WPI), 5-1-5 Kashiwanoha, Kashiwa, Chiba 277-8583, Japan
[2]Department of Physics, ETH Zurich, Wolfgang Pauli Strasse 27, 8093 Zurich, Switzerland
[3]The Inter-University Centre for Astronomy and Astrophysics, Post Bag 4, Ganeshkhind, Pune 411007, India
[4] dominikz@phys.ethz.ch
Draft version February 13, 2019

ABSTRACT

We present evidence for the existence of the splashback radius in galaxy clusters selected using the Sunyaev-Zeldovich effect, a sample unaffected by systematics related to cluster finding in the optical wavelength range. We show that the deprojected cross-correlation of galaxy clusters found in the Planck survey with galaxies detected photometrically in the Pan-STARRS survey, shows a sharp steepening feature (a logarithmic slope steeper than -3), which we associate with the splashback radius. We infer the three-dimensional splashback radius for the SZ cluster sample to be $r_{\rm sp} = 1.85^{+0.26}_{-0.30}\ h^{-1}$Mpc, where the cluster sample has an average halo mass $M_{500\rm c} = 3.0 \times 10^{14} h^{-1} {\rm M}_\odot$ at an average redshift of $z = 0.18$. The inferred value of the splashback radius appears consistent with the expected location for dark matter halos in the standard cold dark matter paradigm. However, given the limited precision of our measurements, we cannot conclusively confirm or rule out the smaller splashback radius measured so far in the literature for optically selected galaxy clusters. We show that the splashback radius does not depend upon the galaxy magnitude for galaxies fainter than $M_i - 5 \log h = -19.44$, and is present at a consistent location in galaxy populations divided by color. The presence of the splashback radius in the star-forming galaxy population could potentially be used to put lower limits on the quenching timescales for galaxies. We can marginally rule out the contamination of the star-forming galaxy sample by quenched galaxies, but the results would need further verification with deeper datasets.

1. INTRODUCTION

The density distribution of matter within dark matter halos shapes the potential well in which galaxies form and grow. Therefore, the structure of these dark matter halos has been extensively studied both theoretically as well as in numerical simulations (see e.g., **?????**). Studies with numerical simulations show that the density profiles of dark matter halos within their virial radii are roughly self-similar and follow the Navarro-Frenk-White (NFW) profile (**?**), which asymptotes to a slope of -1 in the inner regions and -3 at large radii. There has been intense debate in the literature about the exact form of the density profile (e.g., **?**), the value of the asymptotic inner slope, as well as the outskirts and boundaries of dark matter halos (**???**).

The recent study of **?** has sparked a renewed interest in understanding the structure of dark matter halos on scales beyond the typical virial radii. **?** investigated the outskirts of dark matter halos in numerical simulations and found the existence of a physical feature, namely a sharp steepening in the density distributions of dark matter halos, which is not captured by commonly used functional forms such as the NFW profile. They showed that even for halos of the same mass, the position of the feature changes depending upon the mass accretion rate of the halos. A simple theoretical toy model to explain this feature was presented by **?**. They showed that the feature observed by **?** results from the piling up of recently accreted dark matter particles at the apocenters of their orbits, and its location corresponds to the last density caustic in the self-similar models of secondary infall (**???**). They coined the term "splashback radius" for this feature. Their toy model also naturally explains the accretion rate dependence –

This work was submitted and defended as a Masters thesis by Dominik Zuercher at the DPHYS in ETH Zurich in June 2018.

faster accreting halos have smaller splashback radii. Subsequently, **?** suggested the use of the splashback radius as a natural boundary for dark matter halos and explored its consequences for the inferred boundaries and growth rates of the halos. Depending on the accretion rate of the halo, the splashback radius can lie well beyond the commonly used virial radius (**??**).

The interpretation of the accretion rate dependence is straightforward. Due to the continuous change of the gravitational potential of the halo, depending on its accretion rate, the kinetic energy of a recently accreted dark matter particle, gained during its infall onto the cluster, does not suffice to climb the deepened potential well completely again, but instead it "splashes back" at a distance that depends on the recent deepening of the potential well.

Given the mass of the halo, the location of the splashback radius constitutes a direct probe of the halo accretion rate. Motivated by these studies, **?** attempted to detect this feature in observations. Using the optically selected Sloan Digital Sky Survey RedMaPPer galaxy cluster catalog (**?**), and by cross-correlating it with the SDSS photometric galaxy sample, **?** found evidence for the steepening of the dark matter density profile, and therefore the splashback radius of this sample of galaxy clusters. This was corroborated by including further models for mis-centering by **?** and in the Dark Energy Survey data by **?** using optically selected clusters. Somewhat surprisingly, **?** found that the location of the splashback radius was inconsistent with that expected from numerical simulations of dark matter by about $20 \pm 5\%$ (see also **??**). Although they investigated potential systematic issues, they did not have access to mock cluster catalogs which could mimic the selection effects of optically-identified clusters. **?** used a simplified optical cluster selection algorithm on the Millennium simulation, and pointed out that optical clusters can be

heavily affected by projection issues, and could potentially introduce systematics in the inference of the splashback radius, as well as halo assembly bias. The existence of projection effects in the optical cluster catalog in the context of halo assembly bias was also demonstrated by **?**. Regardless of the projection issues present in the optical cluster catalog, there is some inherent circularity present in the logic of using photometric galaxies to select clusters as over-densities in a given aperture, and then using the same photometric sample of galaxies to look for the splashback radius. There is a possibility that the aperture used to select the cluster catalogs could be imprinted in a non-trivial way on the measured number density profiles of clusters.

To avoid such optical cluster selection effects, there have been some previous efforts to use X-ray selected cluster samples to look for the splashback radius using the weak lensing signal (??). However stacking issues and the low signal-to-noise ratio remains a significant hurdle for both of them. **The use of weak lensing data in these studies could get around the biased nature of the galaxy distribution by directly probing the dark matter distribution. Along those lines, ?** found evidence for the splashback feature in the weak lensing signal, but their analysis was again done using optically selected clusters in the Dark energy survey that suffer from the afore-mentioned issues.

In this work, we explore clusters selected using the SZ effect. While the SZ selected clusters can also be susceptible to systematic selection effects, the scales on which the SZ signal is measured and the cluster selection is performed is much smaller than the expected location of the splashback radius (typically R_{500c}). We use this sample to explore the evidence for the splashback radius in observations. Due to the low signal-to-noise ratio of the weak lensing signal, we perform our analysis using cross-correlation of galaxies with clusters.

Dynamical friction is expected to slow down massive subhalos, hosting galaxies that are orbiting the galaxy cluster (?). If a majority of the observed galaxies are hosted by these massive subhalos, the slow down due to dynamical friction would reduce the apocenters of their orbits, and in turn, biasing the measured splashback radius of the host cluster (??). As dynamical friction timescales are inversely proportional to the mass of the subhalos, this effect is stronger for more massive subhalos. Therefore, one expects the splashback radius to decrease for more massive subhalos (?). This bias can be limited by choosing a faint galaxy sample such that the majority of the galaxies reside in low mass subhalos, unaffected by dynamical friction. The SDSS sample used by **?** was already deep enough such that biases in the location of the splashback radius due to dynamical friction effects were expected to be small. Nevertheless, we use galaxy samples, which are fainter by $0.5 - 1$ magnitudes compared to those used by **?**.

Given that the splashback radius represents a true halo boundary, the observations of the splashback radius can be used to study a variety of galaxy formation questions. Questions regarding the timescales and the spatial scales within which star forming galaxies quench after they fall into the cluster potential are of particular interest to understand the fate of star formation in satellite galaxies. In particular, if star forming galaxies quench before they reach the apocenters of their orbit after infall, then they are not expected to show a splashback feature in their density distribution. In pursuit of this question, we also explore the dependence of the

Table 1
Comparison of the PSZ2 cluster catalog against the RedMaPPer cluster catalog used by **?**. The values of the mass estimates M_{500c}, M_{200m}, redshifts z and expected splashback radii $r_{\rm sp}^{\rm 3D,theo}$ represent the catalog averages. The redshifts for both catalogs are given from the survey. For the RedMaPPer catalog the M_{200m} mass estimates were obtained from gravitational lensing and for the PSZ2 catalog the M_{500c} estimates were calculated from the survey parameters using the scaling relation between the integrated Compton Y-parameter Y_{500c} and M_{500c} as found by **?**. The missing mass estimates as well as the expected values of the splashback radii were calculated using the Python package COLOSSUS (**?**). The predictions for the splashback radii $r_{\rm sp}^{\rm 3D,theo}$ are given in comoving units.

	RedMaPPer	PSZ2
z	0.24	0.177
# objects	8643	596
M_{500c} $[h^{-1}10^{14}{\rm M}_\odot]$	0.9	3.0
M_{200m} $[h^{-1}10^{14}{\rm M}_\odot]$	1.8	6.2
$r_{\rm sp}^{\rm 3D,theo}$ $[h^{-1}$ Mpc]	1.37	1.89

cluster-galaxy cross-correlations separately for star forming and quenched galaxy populations as separated by their color.

This paper is organized as follows. We introduce the observational data sets we use in Section **??**, namely the cluster and the galaxy catalogs. We describe the methods and analysis procedures we use in Section **??**. We present and discuss our results in Section **??**. Finally, we summarize our findings in Section **??** and discuss possible future directions. Throughout the paper, we use a flat ΛCDM cosmology with $\Omega_{\rm m} = 0.27$ and a dimensionless Hubble parameter of $h = 0.7$ to convert redshifts and angles into cosmological distances. Also, we denote three-dimensional distances by r and projected distances by R.

2. DATA

In order to avoid optical cluster selection effects, the aim of this paper is to find observational evidence for the existence of the splashback radius in galaxy clusters which have not been selected using optical photometry. To move away from the optical selection we use galaxy clusters selected using the Sunyaev-Zeldovich effect. We describe the data we use in this section.

2.1. *Cluster catalog*

The baryonic component of a galaxy cluster is dominated by the hot, ionized intra-cluster medium (ICM), which is gravitationally bound within the cluster. The cosmic microwave background (CMB) photons that pass through the cluster inverse Compton scatter off the hot electrons and gain energy. This effect is known as the thermal Sunyaev-Zeldovich (SZ) effect (**??**). The effect has a characteristic frequency dependence and results in an intensity decrease below 220 GHz and an associated increase at higher frequencies. The multiple frequency channels on the Planck satellite allow a detection of galaxy clusters using the SZ effect (**?**). As part of the 2015 Data Release of the Planck mission, the second Planck Catalogue of Sunyaev-Zeldovich Sources (PSZ2) was made available to the community. The PSZ2 catalog contains detections based on three different techniques (**?**), and the union of these catalogs has in total 1653 galaxy clusters, of which 1203 clusters have been confirmed by cross-matching to other galaxy clusters from external data sets.

The 1-σ errors on the cluster positions are $\sim 1.6'$ and the estimated purity of the catalog has a lower limit of 83% (**?**). The integrated Compton Y-parameter Y_{500c} of each of the clusters are also provided. The mass estimates M_{500c} provided by the

Table 2
Summary and comparison of the properties of the galaxy catalogs used in this work as well as the SDSS catalog used in **?**.

	SDSS	PS 21	PS 21.5	PS 22
depth [mag]	21.00	21.00	21.50	22.00
eff. area [deg^2]	$\approx 10,000$	21,148	20,586	15,689
# objects	57,181,113	93,772,329	123,188,529	105,809,113
objects/deg^2	5718	4434	5984	6744

Planck collaboration are based on the scaling relation between Y_{500c} and M_{500c} (**???**). The PSZ2 union cluster catalog is publicly available from the *Planck Legacy Archive*[1].

We restrict ourselves to the redshift range $0.03 \leq z \leq 0.33$ in order to have a similar redshift range as used in **?**. Due to the larger beam size of the Planck satellite, the cluster positions as reported in the catalog may be mis-centered from the true centers of the galaxy clusters. We perform a visual inspection of Pan-STARRS images taken around the detected galaxy clusters in order to locate the nearest, brightest cluster galaxy (BCG). We regard the position of the BCG as the true cluster location, under the assumption that the BCG is located at the true, gravitational center. Due to this assumption, we additionally study the effects of a possible, remaining mis-centering of the cluster positions in our model for the two-dimensional correlation function (see Appendix **??**).

The final sample that we use consists of 596 galaxy clusters and is about an order of magnitude smaller compared to the sample used in **?**. The sample we use in this paper has an average redshift of 0.177, and an average cluster mass M_{500c} of about $3.0 \times 10^{14} h^{-1} M_{\odot}$. In Table **??** we compare the main properties of the cluster catalog used in this work to that used by **?**. Additionally, Figure **??** visualizes the distribution of the masses and redshifts of the used clusters. A map of the sky positions of the clusters as well as a visualization of their redshift and mass distributions can be found in Appendix **??**.

? found no evidence for a significant correlation between the density of Planck detections and the weighted average noise of all Planck channels at $z < 0.5$. Since we restrict ourselves to $z < 0.33$, we utilize the selection mask of the PSZ2 union catalog in order to construct a random galaxy cluster catalog, which is roughly one order of magnitude larger than the original catalog. The redshifts of these random objects are drawn from the parent cluster catalog in order to match the redshift distribution of the original cluster catalog.

2.2. *Galaxy catalog*

The Panoramic Survey Telescope and Rapid Response System (Pan-STARRS) is a wide-field astronomical imaging and data processing facility operated by the University of Hawaii's Institute for Astronomy (**??**). We use data from the 3π Steradian Survey carried out with this facility, which was released as part of Data Release 1 (DR1). The survey covers the entire sky north of $\delta = -31°$ (in ICRS coordinates) in five broadband filters ($g_{P1}, r_{P1}, i_{P1}, z_{P1}, y_{P1}$) with multiple pointings. The mean 5σ point source limiting sensitivities amount to (23.3, 23.2, 23.1, 22.3, 21.4) magnitudes for the individual bands, respectively.

For the visual inspection and centering of the clusters, we use the Pan-STARRS *gri stack* images around each cluster position. The galaxy catalog is obtained from the *StackObjectThin* table, which is publicly available on the *Barbara A. Mikulski Archive for Space Telescopes* (MAST)[2]. To select

only objects detected with acceptable precision we restrict our search to those objects which have been flagged as *BestDetection*s. We further restrict the catalog to objects flagged as *PrimaryDetection*s in order to select unique objects. This is necessary since the survey is divided into overlapping *projectioncells* and *skycells*, which causes some objects to be listed multiple times.

The magnitudes of the selected objects are then corrected for the extinction caused by dust present in the Milky Way. This is done using the mwdust[3] Python module provided by **?**. The extinction correction is performed using a dust map combining the measurements of **?**, **?** and **?**. Only objects with an extinction corrected i_{P1} band Kron magnitude brighter than 22.0 are selected from the catalog. Starting from this catalog we construct three different sub-catalogs corresponding to survey depths of 21.0, 21.5 and 22.0 magnitudes, and we name these catalogs PS 21, PS 21.5 and PS 22, respectively.

As mentioned in the description of the Pan-STARRS survey by **?** there is a significant variation in the depth of the 3π Steradian survey even on small scales. In order to avoid choosing objects in shallow regions of the survey the maximum observed Kron magnitude in the i_{P1} band in each *skycell* is recorded and only objects in skycells with a maximum observed Kron magnitude of 21.0, 21.5 and 22.0 or brighter are selected depending on the corresponding catalog. Since most of the shallow regions lie in the galactic plane, we mask out the region at low galactic latitudes $|b| < 20°$. The resultant HEALPix maps showing the excluded areas on the sky can be found in Appendix **??**. We further disregard objects in bad pixel regions as indicated by the i_{P1} band *stack.mask* images.

At this point of the analysis, our object catalogs contain both galaxies and stars. The 3π Steradian Survey provides both the Kron and PSF model based magnitudes for each object. These magnitudes are expected to be similar for stars while the Kron magnitudes are brighter for galaxies. Therefore, we flag all objects with a value of $i_{P1,PSF} - i_{P1,Kron} < 0.05$ as stars (**?**). Despite this cut, bright, close-by stars at magnitudes brighter than 13.5 tend to be classified as extended objects (**?**). To avoid contamination of the galaxy catalog due to such bright stars, we further remove all objects with $i_{P1,PSF} < 15.0$. Since there are very few galaxies at such low magnitudes this does not introduce a selection bias. We list the main characteristics of the galaxy catalogs we have used in Table **??**.

3. METHODS

The methodology we adopt for locating the splashback radius closely follows that of **?**. We perform a cross-correlation between SZ selected galaxy clusters with photometric galaxies in order to assess the existence and location of the splashback radius. We use the Davis-Peebles estimator (**?**) to compute the cross-correlation between our galaxy clusters and

---

[1] https://pla.esac.esa.int/pla/#home
[2] http://archive.stsci.edu/

[3] https://github.com/jobovy/mwdust

galaxies. This estimator can be written as

$$\xi_{2D}(R) = \frac{D_1 D_2 - R_1 D_2}{R_1 D_2} \quad (1)$$

where $D_1 D_2$ and $R_1 D_2$ are the normalized numbers of cluster-galaxy pairs and cluster randoms-galaxy pairs at a given co-moving projected separation R. The subtraction of the signal around random cluster positions gets rid of the uncorrelated pairs and allows us to estimate the projected cross-correlation. The uncertainty in the galaxy distribution masks prevents us from using the Landy-Szalay estimator (**?**).

Given the flux limited galaxy catalog that we use, we expect to observe more correlated galaxies in galaxy clusters that lie closer to us, but with much fainter absolute magnitudes. To avoid such biases with redshift of the clusters we restrict ourselves to galaxies with absolute magnitudes brighter than a certain magnitude limit, which depends on the depth of the used galaxy catalog. We make the assumption that the galaxies reside at the redshift of the cluster in question. The magnitude limits we use are -19.44, -18.94 and -18.44 and name the corresponding catalogs PS 21, PS 21.5 and PS 22, respectively.

We use the functional form of **?** in order to model our two-dimensional correlation function measurements. This functional form consists of an inner Einasto profile and an outer power law profile connected by a smooth transition

$$\xi_{3D}(r) = \rho_{in}(r) f_{trans}(r) + \rho_{out}(r), \quad (2)$$

$$\rho_{in}(r) = \rho_s \exp\left(-\frac{2}{\alpha}\left[\left(\frac{r}{r_s}\right)^\alpha - 1\right]\right), \quad (3)$$

$$\rho_{out}(r) = \rho_0 \left(\frac{r}{r_{out}}\right)^{-s_e}, \quad (4)$$

$$f_{trans}(r) = \left(1 + \left(\frac{r}{r_t}\right)^\beta\right)^{-\gamma/\beta}, \quad (5)$$

where r indicates the three-dimensional radial distance from the halo center (**?**). We model the two-dimensional correlation function, ξ_{2D} as an integral over the three-dimensional correlation function

$$\xi_{2D}(R) = \frac{1}{R_{max}} \int_0^{R_{max}} \xi_{3D}(\sqrt{R^2 + x^2}) dx \quad (6)$$

where we adopt $R_{max} = 40\ h^{-1}$Mpc for the maximum projection length. Variations of this length do not change the location of the splashback radius appreciably as tested in **?**. The functional form adopted in Equation **??** has nine model parameters, $\rho_s, \alpha, r_s, r_{out}, \rho_0, s_e, r_t, \beta$ and γ. Given the perfect degeneracy between the parameters r_{out} and ρ_0, we fix $r_{out} = 1.5$ h^{-1}Mpc.

Therefore the model is described by eight model parameters. We infer the posterior distributions of those parameters by fitting the model for the two-dimensional correlation function to the measured two-dimensional correlation signal. We use the affine invariant Markov Chain Monte Carlo sampler of **?** as implemented in the parallel python package *emcee* by **?**. **We let the parameters ρ_s, ρ_0 and s_e vary freely during our fitting procedure. Similar to ? we put flat priors on $\log_{10}(r_s)$ and $\log_{10}(r_t)$ but double their ranges to [0.1, 5.0] compared to their work. In contrast to ?, we use a normal prior with a central value of $\log_{10}(0.2)$ and a scale of 1.2 for $\log_{10}(\alpha)$ as deduced from mass estimates (?). For the parameters $\log_{10}(\beta)$ and $\log_{10}(\gamma)$ we also use normal priors**

with central values $\log_{10}(6.0)$ and $\log_{10}(4.0)$, respectively and scale 0.4 as recommended by ?.

It has been a common concern that the profile in Equation ?? introduces a point of minimum slope in the logarithmic derivative profile simply due to the functional form. However, ? used a Bayesian evidence approach to assess that the data is described significantly better by the general profile in Equation ?? (with the splashback feature) rather than by the same profile with fixed $f_{trans} = 1$ (without splashback feature). The same conclusion was made by ? who conducted a similar study but using weak lensing data.

The location of the splashback radius can be identified in various ways, e.g., as the radius of the outermost shell in theoretical models of spherical symmetric collapse (??), or using non-spherical shells of density jumps (?), or the average location of the apocenter of particles falling in the cluster potential ?. Although these definitions have subtle differences, they all follow the general trend of a decreasing splashback radius with increasing rate of accretion (?). In this paper, we adopt the convention of ?, who define the location of the splashback radius for halos on galaxy cluster scales to be the location of the steepest logarithmic slope of the radially averaged density profile, due to its ease of accessibility in data.

We estimate the steepest slope of both the two-dimensional and the three-dimensional cross-correlation function. The locations of the steepest slope in the two-dimensional and the three-dimensional case are expected to be different by about 20% for typical cluster halo parameters (**??**).

Mis-centering of the central cluster positions can affect the small-scale correlation function on scales smaller than the typical mis-centering distance. Although, the splashback radius is located at much larger scales, the change of the inner part of the correlation function can alter the model fit significantly. Mis-centering effects are not expected to change the location of the splashback feature but they can in principle decrease the significance of the evidence for the splashback feature (**?**). We discuss the modelling of mis-centering and its effects on the inferred splashback radii in Appendix **??**.

3.1. *Separation of red and blue galaxies*

We are also interested in measuring the cluster-galaxy cross-correlations for the blue and the red galaxy samples separately. We use a $g_{P1} - r_{P1}$ color cut which varies with the redshift of the clusters in order to account for the k-corrections, which cannot be computed individually for each galaxy.

In order to compute the color cut to be used, we first match spectroscopic galaxies in the Sloan Digital Sky Survey (DR 8) to their Pan-STARRS photometry. We bin these galaxies in narrow redshift bins and produce a histogram of the $g_{P1} - r_{P1}$ colors of the galaxies in each bin. Due to the presence of the 4000Å-break present in the quenched galaxy population, the two galaxy populations separate in such histograms into two populations and we fit a double Gaussian distribution to it. Based on the fitted distribution we use a cut in color to exclude a contamination to the star-forming galaxy population with a confidence of 3σ. We repeat this procedure for each redshift bin, to obtain a redshift dependent color cut that separates the red from the blue population minimizing the contamination of the blue population by red galaxies. Although being much simpler and faster than calculating the individual k-corrections for each galaxy, this procedure has its own

shortcomings as discussed in Appendix **??**, in particular due to the photometric errors of red galaxies. We would therefore exercise appropriate caution while interpreting the results obtained by dividing galaxies into color bins.

In our analysis, the same galaxy may be considered red or blue depending upon the cluster redshift under consideration. Our method avoids the use of uncertain photometric redshifts to derive k-corrections (cf. **?**). We will study the cross-correlations to derive the splashback radii for these galaxy populations separately. The caveats in the interpretation of these results due to photometric errors are discussed in the Appendix **??**.

4. RESULTS

The measurements of the two-dimensional cluster-galaxy cross-correlations are shown as black points with error bars in the first row of Figure **??**. The different columns correspond to the three different absolute magnitude limits that we have used to select all the galaxies when calculating the cross-correlations. The cross-correlation signal is clearly detected in all three measurements. **The signal to noise ratios of the three different estimates of the two-dimensional cross-correlation signals amount to 42.4, 43.3 and 30.9 for the galaxy samples PS 21, PS 21.5 and PS 22, respectively. For comparison, the detection SNR in ? was 263, a much higher number due to the size of the cluster sample used in their study.**

We fit these measurements with our parametric model in Equation **??** and compute the posterior distribution of the model parameters as described in Section **??**. The median of the MCMC fit is indicated by the central solid line, while the shaded area marks the 68% credible interval for the fit. The median values of the posterior distributions of the parameters along with their 68% confidence intervals are listed in Table **??** along with the corresponding reduced χ^2 values for the best fit.

We show the two-dimensional posterior distributions for each pair of parameters for the PS 21.5 sample in Figure ??. The posterior distributions for the other datasets show similar degeneracies and are not included in the paper for brevity. It is observed that there are some strong degeneracies present between parameters describing the same part of the model in Equation ?? (namely ρ_{in}, f_{trans} and ρ_{out}). This is expected since certain combinations of parameter values can very well result in the same functional shape of the different parts of the model. This degeneracy also leads to some of the parameters not being constrained tightly (especially ρ_s and r_s due to their strong degeneracy with α). On the other hand, it is important to note that there is little-to-no degeneracy present between parameters describing different parts of the model, which means that the overall shape of the profile is well constrained. Note also that, since the location of the splashback radius only depends on the overall shape of the profile, the uncertainties of the individual parameters within the independent parts of the profile do not translate into a huge uncertainty on the location of the splashback feature.

The second row in Figure **??** shows the corresponding analytical derivatives of the two-dimensional cross-correlations and the 68% confidence interval based on our model fits. The logarithmic derivatives show a distinct steepening feature at around 1.3 h^{-1}Mpc. The figure shows that the location of the steepest slope does not change appreciably when the magnitude limit is changed, even though we use a sample which

is one magnitude fainter than $M_i - 5 \log h = -19.44$. The 68% confidence interval of the location of the steepest slope is indicated by the vertical, shaded region. We also show the location of the virial radius r_{200m} based on the Planck SZ mass estimate as a black, dotted line in each panel.

We use the posterior distributions of our model parameters to infer the three-dimensional cross-correlation and its first and second order logarithmic derivatives. These inferences along with the corresponding 68% confidence intervals are presented in the last three rows of Figure **??**. The three-dimensional cross-correlations also show significant steepening in each of the cases that we have explored, reaching logarithmic derivatives steeper than −3. The inferred 68% confidence regions of the locations of the steepest slope of the three-dimensional cross-correlations are shown with vertical, shaded regions in each panel. The posterior distributions of the locations of the steepest slope in the two-dimensional and three-dimensional cross-correlations can be found in the left hand and middle panels of Figure **??**, respectively. The estimates of the splashback radii for each of the samples are listed in Table **??** and our results show that the location of the splashback radius does not depend upon the sample once we use galaxies fainter than $M_i - 5 \log h = -19.44$. Our measurements have an accuracy of ~15%.

Following **?**, we also present the values of the first order logarithmic derivatives at the location of the steepest slope for the total three-dimensional cross-correlations in the right hand panel of Figure **??**. The logarithmic slope of the cross-correlation is significantly steeper than −3 at the location of the splashback radius, making it difficult to be reproduced by classical fitting functions like the NFW profile, which reach such slopes only asymptotically and even that only without the presence of the outer 2-halo term. This provides evidence for the existence of the splashback feature. From the second order derivative profiles we also note that the drop in the cross-correlation signal is very sharp and happens within a factor 2 in radius.

We perform a preliminary comparison of the measurements with expectations from cold dark matter models. The average halo mass of the PSZ2 clusters as estimated from the Sunyaev-Zeldovich signal is $M_{500c} = 3.0 \times 10^{14} \ h^{-1}M_\odot$. We convert this mass estimate to $M_{200m} = 6.2 \times 10^{14} \ h^{-1}M_\odot$ using the average concentration mass relation of halos assuming an NFW profile (**?**). Given the average mass and redshift of our cluster sample, we calculate the expected splashback radius to be 1.89 h^{-1}Mpc. We base this estimate on the fitting functions presented in **?**. The splashback radius we find for the three samples is consistent with this expectation, although we can not rule out ~ 15% deviations in either directions, given our large error bars.

Next, we present our measurements of the projected and three-dimensional cross-correlations of the red and blue galaxy populations satisfying $M_i - 5 \log h < -18.94$ with our SZ-selected cluster sample. The projected cross-correlations as well as the three-dimensional counterparts are shown in Figure **??**. The shaded regions show the 68% confidence intervals from our fits. The vertical, shaded bands with different colors indicate the 68% confidence regions of the locations of the steepest slope of the two- and the three-dimensional cross-correlations. The black dashed lines show these ranges for the entire galaxy sample without regard to color. The best fit parameters as well as the inferred splashback radii are listed in Table **??**. We see that the red galaxies have a steeper cross-correlation profile than the blue galaxies. Although there
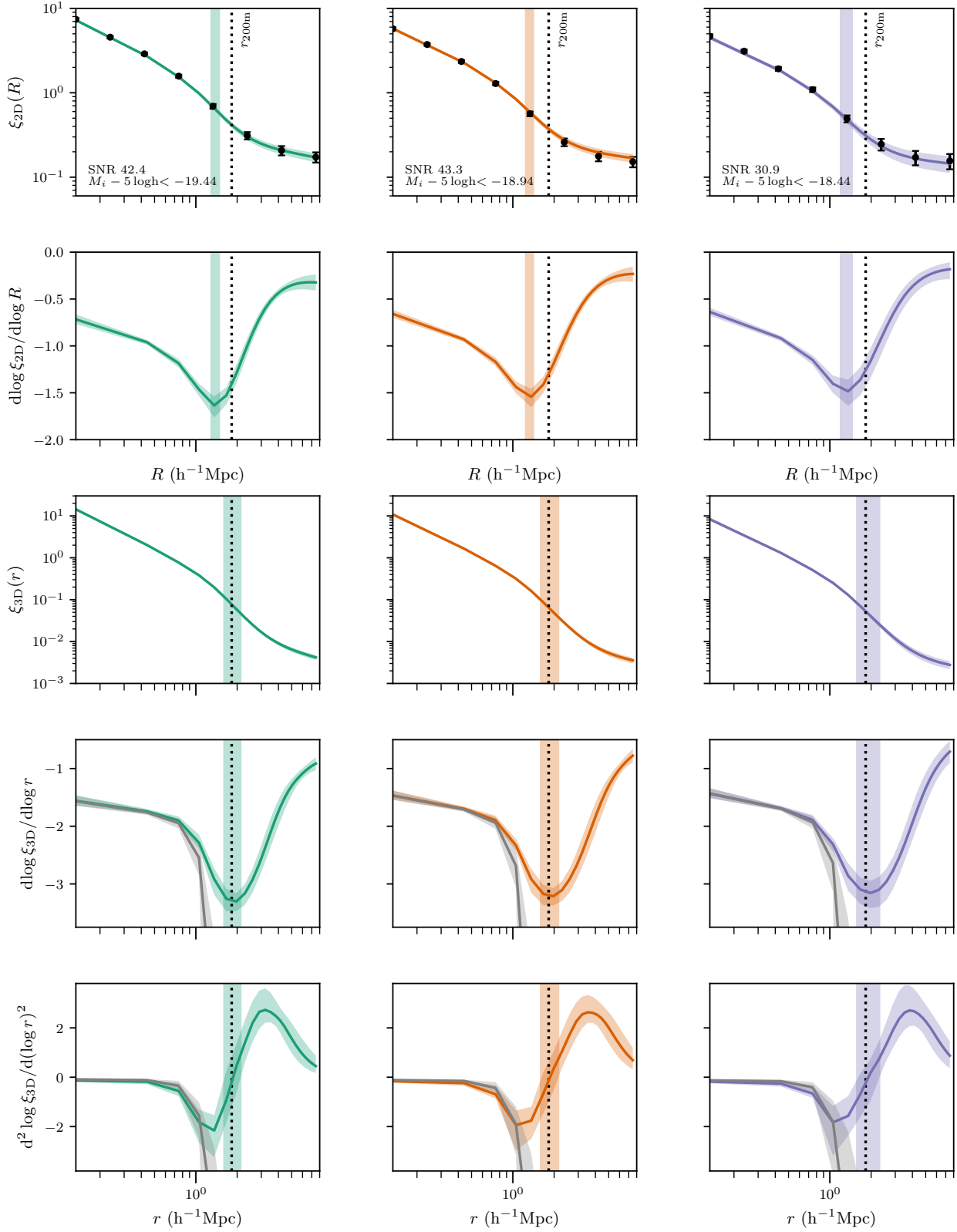
Figure 1. The main results of the study are presented in this Figure. The first two rows show the inferred two-dimensional cross-correlation signals as well as its derivatives. The three different columns correspond to the three different galaxy samples cross-correlated with the cluster sample. The magnitude limit applied to the galaxy catalog is indicated in each tile of the first row along with the signal-to-noise ratio (SNR). The measurements of the two-dimensional cross-correlation signals (black dots) are shown in the first row as well. There, the colored curves show the two-dimensional model fits of the functional form in Equation **??**. The vertical, shaded regions indicate the estimates of the locations of steepest slope of the profiles as estimated from the corresponding minima of the two-dimensional derivative profiles, which are shown in the second row. Rows three to five show the corresponding three-dimensional model fit with the functional form Equation **??** as well as its first and second order derivatives. In rows three to five the vertical, shaded regions indicate the estimates of the splashback radii as estimated from the corresponding minima of the three-dimensional derivative profiles. The grey curves show the corresponding, estimated first and second derivatives of the one-halo term (namely $\rho_{in}(r)f_{trans}(r)$ in Equation **??**). For comparison, the location of the r_{200m} radius as calculated from the average cluster sample properties is indicated by the black, dotted lines.

Table 3
The Table presents the posterior distribution of the parameters obtained from fitting the cross-correlation of the galaxy cluster sample with the different galaxy catalogs. For each parameter estimate the median as well as the 16% and 84% quantiles of the posterior distribution are given. We also list the estimated locations of the steepening feature in the two-dimensional cross-correlation signal (R_{sp}^{2D}), as well as the three-dimensional splashback radius (r_{sp}^{3D}). In the last column the minimum, reduced χ^2 value of the model fit is indicated.

| gal cat	$\log_{10}(\rho_s)$	$\log_{10}(\alpha)$	$\log_{10}(r_s)$	ρ_0	s_e	$\log_{10}(r_t)$	$\log_{10}(\beta)$	$\log_{10}(\gamma)$	R_{sp}^{2D}	r_{sp}^{3D}	χ^2/ν
PS 21	$-2.93^{+0.44}_{-0.50}$	$-1.06^{+0.14}_{-0.18}$	$0.35^{+0.27}_{-0.24}$	$0.000179^{+0.000075}_{-0.000086}$	$0.78^{+0.24}_{-0.19}$	$0.123^{+0.051}_{-0.122}$	$0.74^{+0.21}_{-0.31}$	$0.35^{+0.13}_{-0.21}$	$1.384^{+0.088}_{-0.096}$	$1.86^{+0.25}_{-0.26}$	1.524
PS 21.5	$-2.93^{+0.45}_{-0.45}$	$-0.95^{+0.13}_{-0.16}$	$0.32^{+0.25}_{-0.25}$	$0.000103^{+0.000047}_{-0.000065}$	$0.56^{+0.25}_{-0.22}$	$0.095^{+0.045}_{-0.115}$	$0.74^{+0.24}_{-0.32}$	$0.27^{+0.12}_{-0.19}$	$1.323^{+0.080}_{-0.086}$	$1.85^{+0.26}_{-0.30}$	0.285
PS 22	$-2.95^{+0.49}_{-0.44}$	$-0.91^{+0.14}_{-0.17}$	$0.28^{+0.25}_{-0.27}$	$0.000062^{+0.000028}_{-0.000051}$	$0.41^{+0.25}_{-0.28}$	$0.094^{+0.060}_{-0.190}$	$0.76^{+0.29}_{-0.36}$	$0.24^{+0.14}_{-0.27}$	$1.31^{+0.11}_{-0.14}$	$1.90^{+0.32}_{-0.40}$	0.211
PS 21.5 (R)	$-0.69^{+0.55}_{-0.54}$	$-0.99^{+0.17}_{-0.20}$	$0.24^{+0.30}_{-0.31}$	$0.0092^{+0.0046}_{-0.0065}$	$0.63^{+0.30}_{-0.27}$	$0.157^{+0.091}_{-0.171}$	$0.54^{+0.16}_{-0.20}$	$0.36^{+0.17}_{-0.26}$	$1.437^{+0.099}_{-0.089}$	$2.13^{+0.22}_{-0.21}$	0.502
PS 21.5 (B)	$-1.00^{+0.47}_{-0.24}$	$-0.31^{+0.21}_{-0.15}$	$0.22^{+0.19}_{-0.31}$	$0.0078^{+0.0036}_{-0.0047}$	$0.52^{+0.24}_{-0.21}$	$0.31^{+0.29}_{-0.27}$	$0.61^{+0.31}_{-0.44}$	$0.30^{+0.29}_{-0.39}$	$1.43^{+0.12}_{-0.13}$	$2.34^{+0.33}_{-0.34}$	1.355
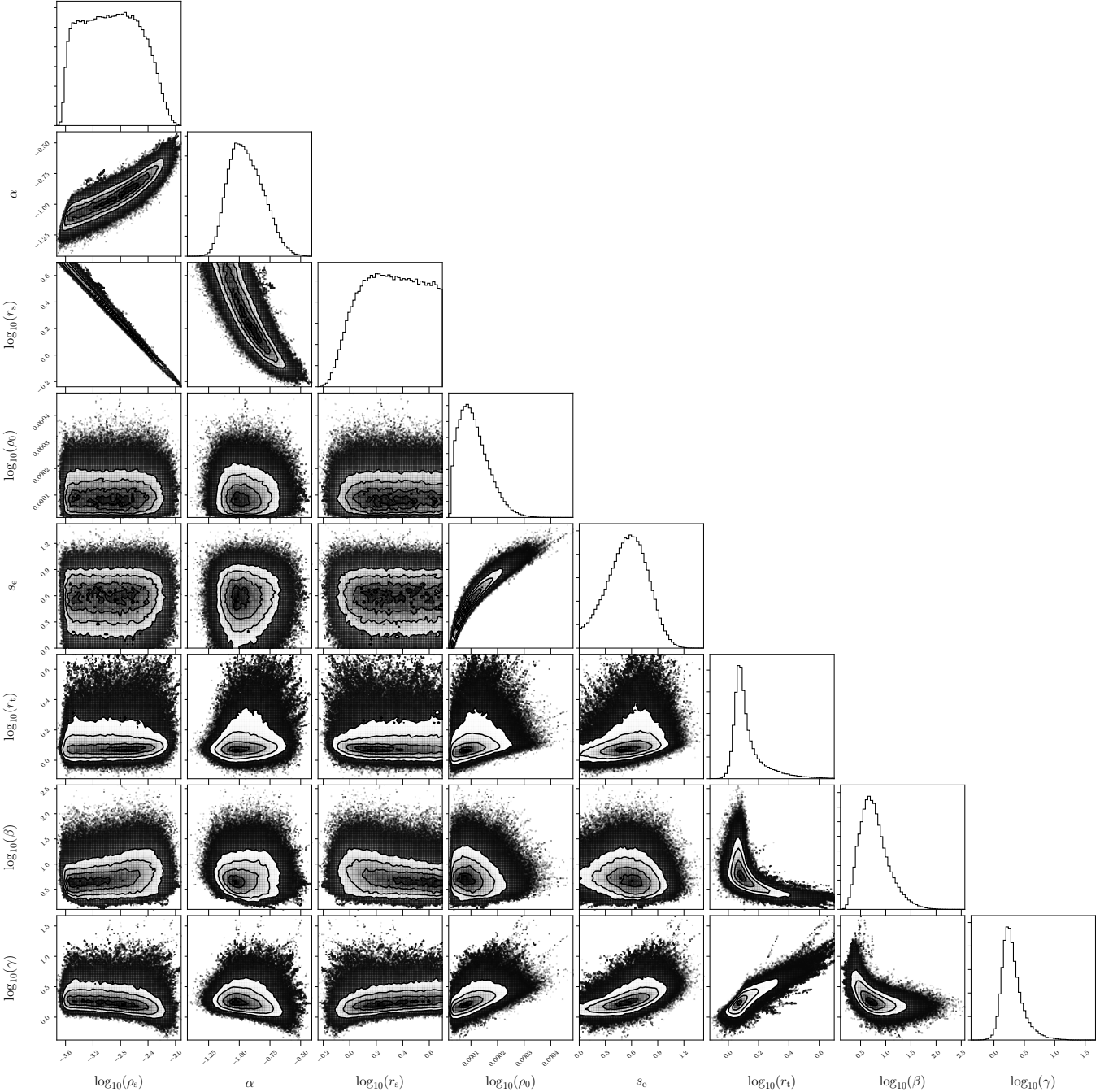
Figure 2. The two-dimensional posterior distributions of each pair of the fitting parameters corresponding to the functional form in Equation **??** for the PS 21.5 sample.
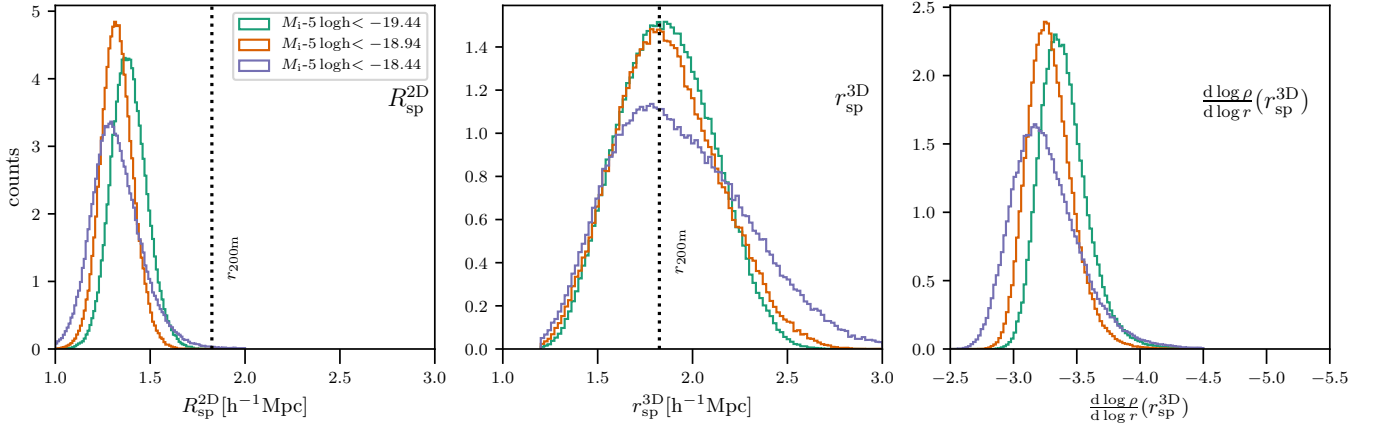
Figure 3. The posterior distributions of the locations of the two-dimensional steepening feature (R_{sp}^{2D}) are shown in the leftmost panel, while the distributions of the three-dimensional counterparts (r_{sp}^{3D}) are shown in the middle one. For comparison, the location of the virial radius r_{200m} as calculated from the average cluster sample properties is indicated by the black, dotted lines. Additionally, the distributions of the logarithmic derivatives of the three-dimensional cross-correlation signals at the location of the splashback radius are shown in the rightmost panel. The magnitude limit applied to the galaxy catalogs is indicated for each distribution. Note that the colors of the distributions match with the colors used in Figure **??**.

seems to be a tendency for the red galaxies to have a smaller splashback radius, the differences we see are not statistically significant given the current errors. The slopes of the three-dimensional cross-correlations reach values steeper than -2.5 at the splashback radius, which is difficult to model with traditional NFW profiles. We take the detection of those steepening features as evidence for the existence of the splashback feature in both galaxy populations. Taken at face value, our finding of the splashback feature in the blue population would imply that there needs to be a reasonable fraction of blue galaxies that fall into the cluster and continue to stay blue even after reaching their apocenters.

This result seem to be at odds with the findings presented by ?, who find no splashback feature in the blue galaxy population. Our investigations suggest that the splashback feature gets less prominent as we proceed to look at galaxies which are progressively bluer in color. Given that ?, consider the last quartile of the blue population, it is imaginable that they see no evidence for the splashback feature in their dataset. The approach used by ? used to separate galaxies into red or blue is also fundamentally different from our approach. While ? use K-corrected magnitudes from SDSS relying on the photometric redshifts of galaxies (which could have different uncertainties for the red and the blue population), we rely on a color cut which depends upon the redshift of the cluster under consideration.

We caution that the cut we use to define our color-separated samples was defined based on spectroscopic galaxies, which tend to be brighter than the typical galaxies we use for the cross-correlation. As we use galaxies at fainter magnitudes for the cross-correlation, the photometric errors increase dramatically and can scatter many more of the red galaxies into the blue galaxy sample. We report on our investigations in Appendix **??** as a cautionary tale, and to guide future efforts to establish the splashback radius in the blue galaxy population. We show that given the current state of the data we can marginally exclude a contamination of the correlation function of blue galaxies from the red galaxy population but appropriate caution is warranted in the interpretation or use of the results derived using the color separated galaxy populations.

5. CONCLUSIONS AND FUTURE DIRECTIONS

The splashback radius of dark matter halos is a unique observational probe of the mass accretion rate of dark matter halos. Although the splashback radius has been well-characterized in simulations, the observational evidence for the splashback radius presented using optical cluster catalogs has come under intense scrutiny. In this work, we tackle this issue by searching for evidence of the splashback radius in galaxy clusters found by the Planck surveyor using the thermal Sunyaev-Zeldovich effect. The use of this sample avoids the circularity of using photometric galaxy catalogs to identify clusters as well as to detect the splashback radius.

We cross-correlate these clusters with photometric galaxies from the Pan-STARRS survey to obtain the two-dimensional cross-correlation function and search for evidence for the splashback feature. Additionally, we divided our galaxy catalog into two subsamples of red and blue galaxies and investigated the cross-correlations of the two subsamples with the clusters, separately.

Our main findings can be summarized as follows:

- We detect a clear signature of a steepening feature in the cross-correlation of Planck SZ clusters with Pan-STARRS galaxies. The steepest logarithmic slopes that we find in our cross-correlation signals are steeper than -3, and would hence be poorly fit by the NFW profile. We associate this steepening with the splashback feature.

- The location of the inferred splashback radius is $r_{sp} = 1.85_{-0.30}^{+0.26} \, h^{-1} \mathrm{Mpc}$, which is consistent with expectations from numerical simulations for halos of an average mass $M_{500c} = 3.0 \times 10^{14} h^{-1} \mathrm{M_\odot}$ at an average redshift of $z = 0.18$ in a collision-less dark matter Universe. However, given the errors we cannot currently rule out $\sim 15\%$ deviations from these expectations.

- We find that the location of the steepest slope does not strongly depend on the magnitude of the galaxy samples we use, once we go fainter than $M_i - 5\log h = -19.44$.
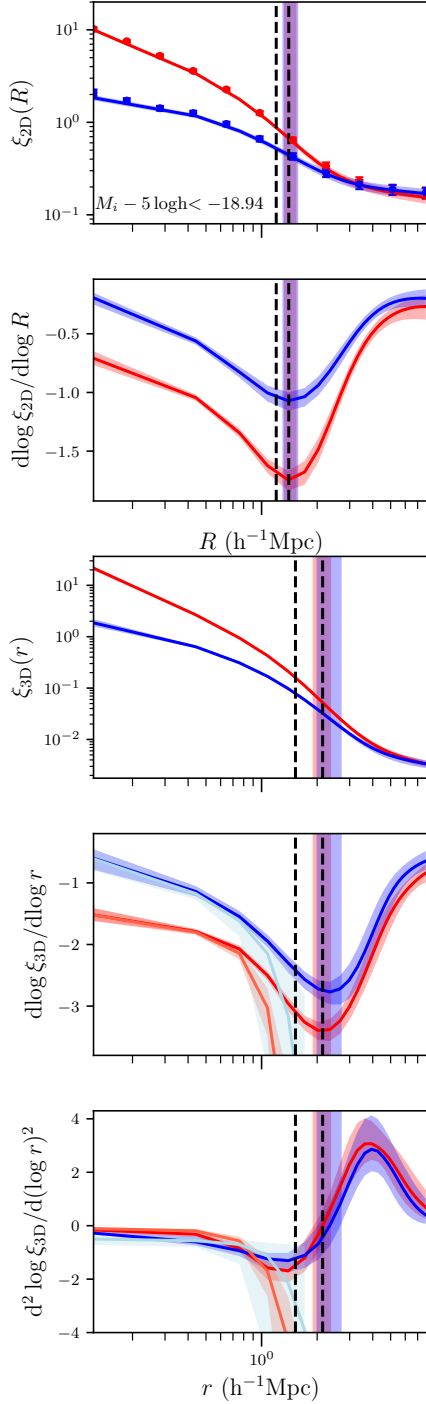
- By separately studying the cross-correlation of red and

Figure 4. We present the cross-correlations inferred for the color-separated galaxy samples. The two-dimensional cross-correlations of the red and blue galaxy populations as inferred by cross-correlating the cluster sample with the color-separated subsamples that were extracted from the PS 21.5 galaxy catalog are shown in the top panel, whereas the associated derivative profiles are shown in the second one. The vertical, shaded bands indicate the locations of steepest slope of the two-dimensional cross-correlation signal as inferred from the two subsamples, whereas the black, dashed lines indicate the upper and lower bounds of the same feature but as estimated from the full PS 21.5 galaxy catalog. Panels three to five show the corresponding three-dimensional cross-correlations, as well as the corresponding splashback radii (indicated by the colored, vertical bands) and their first and second order derivative profiles. The light-colored curves show the corresponding first and second order derivatives of the one-halo term (namely $\rho_{in}(r)f_{trans}(r)$ in Equation **??**). Here, the black, dashed lines indicate upper and lower bounds of the three-dimensional splashback radius corresponding to the full PS 21.5 galaxy sample.

blue galaxies with the clusters, we present evidence for the presence of the splashback feature in both populations. The existence of the splashback radius for the star forming galaxy population could be of significance for the models of satellite quenching in galaxy clusters. However, photometric errors hinder a clean interpretation of the signal.

The signal-to-noise ratio of the current measurement is a result of the limited depth of the Pan-STARRS catalog, as well as the limited number of galaxy clusters detected using the SZ effect. As we consider fainter galaxy catalogs, the sky fraction in which the Pan-STARRS galaxy catalogs are complete reduces. Furthermore, the contamination from background galaxies is expected to increase at deeper magnitudes as well. A more precise estimation of the uncorrelated component would be possible by using a random galaxy catalog in addition to the random cluster sample. The masking information in Pan-STARRS is not currently easily accessible, which prevents the use of the more sophisticated Landy & Szalay estimator. Increasing the redshift range of clusters could potentially yield a bigger cluster sample, but would require us to use a sample of galaxies with a brighter absolute magnitude limit for galaxies, which reduces the number of galaxies that can be used to infer the cross-correlation signal. We are exploring the use of alternative cluster catalogs such as those detected from Xray surveys.

The separation of the blue and red galaxy populations as described in Section **??** is prone to photometric errors as explored in the Appendix **??**. A deeper galaxy catalog would be required in order to confirm or rule out the existence of the splashback feature in the blue galaxy population. The ongoing deep galaxy surveys such as the Hyper Suprime-Cam (**?**) and the Dark Energy Survey (**?**) would be able to provide such data sets, albeit in a limited area. The Large Synoptic Survey telescope (**?**) would eventually provide deep as well as wide galaxy catalogs to eventually establish the locations of the splashback radius at high significance.

Lastly, but most importantly, the investigation of any systematics which might originate from the SZ selection of the Planck clusters is beyond the scope of the current work. We caution that there may be residual systematics in the selection which could affect the interpretation of our measurements. We plan to investigate such selection systematics with the help of hydrodynamical simulations.

Our curated galaxy catalogs from the Pan-STARRS survey for different depths and the corresponding masks are available upon request.

While this work was in preparation, we became aware of a related study by Shin et al. (2018). Our results are complementary to theirs given the different data samples and cluster catalogs.
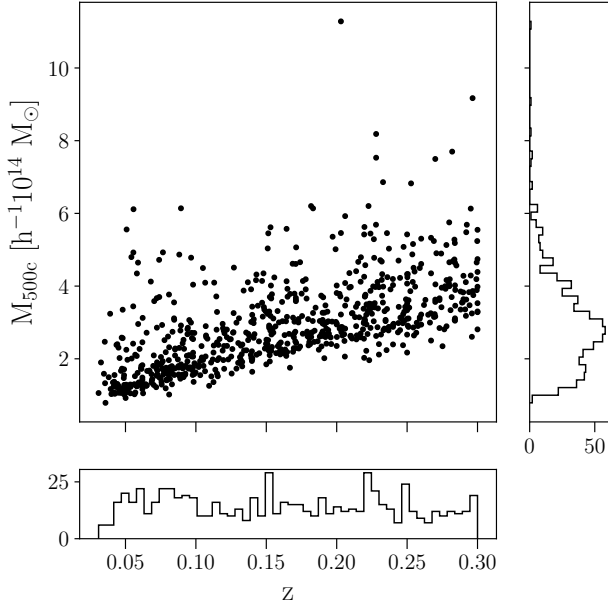
Figure 5. The distribution of the masses and redshifts of the galaxy clusters from the PSZ2 catalog that we use in our analysis. The histograms on the right hand side and the bottom show the distribution in mass and redshift, respectively.

ence archive have been made possible through contributions by the Institute for Astronomy, the University of Hawaii, the Pan-STARRS Project Office, the Max-Planck Society and its participating institutes, the Max Planck Institute for Astronomy, Heidelberg and the Max Planck Institute for Extraterrestrial Physics, Garching, The Johns Hopkins University, Durham University, the University of Edinburgh, the Queen's University Belfast, the Harvard-Smithsonian Center for Astrophysics, the Las Cumbres Observatory Global Telescope Network Incorporated, the National Central University of Taiwan, the Space Telescope Science Institute, the National Aeronautics and Space Administration under Grant No. NNX08AR22G issued through the Planetary Science Division of the NASA Science Mission Directorate, the National Science Foundation Grant No. AST-1238877, the University of Maryland, Eotvos Lorand University (ELTE), the Los Alamos National Laboratory, and the Gordon and Betty Moore Foundation.

Based on observations obtained with Planck (http://www.esa.int/Planck), an ESA science mission with instruments and contributions directly funded by ESA Member States, NASA, and Canada. Some of the results in this paper have been derived using the HEALPix (K.M. Górski et al., 2005, ApJ, 622, p759) package

APPENDIX

A. VISUALIZATION OF THE DATA

We visualize some of the main properties of the used data catalogs. In Fig. **??** we show the mass and the redshift distribution of the Planck clusters. In Figure **??** we present the sky locations of the SZ selected clusters from the PSZ2 catalog that we used in our study (red points). The purple areas mark the masked out regions of the galaxy catalogs. All sky maps presented use the ICRS coordinate system.
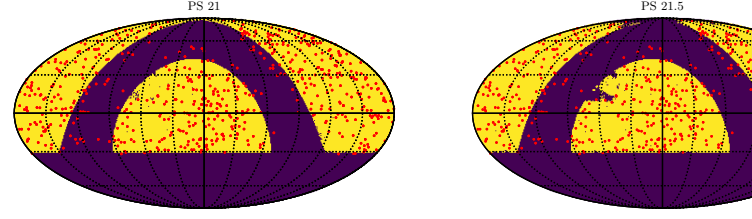

Figure 6. Sky maps showing the sky positions of the used clusters as selected from the PSZ2 catalog. In total 596 clusters have been selected. The purple areas mark the masked out regions of the used galaxy catalogs extracted from the Pan-STARRS 3π Steradian survey. Note that all clusters with $\delta < -31°$ have been removed since this region is not covered by the Pan-STARRS 3π Steradian survey. The ICRS coordinate system is used.

B. MODELLING CLUSTER MIS-CENTERING

As can be seen from the analysis and results in **?**, the mis-centering of the central cluster positions in optical clusters were not large enough to change the location of the steepest slope in the cluster-galaxy cross-correlations. They do however decrease the significance of the finding. Therefore, we explore the effects of mis-centering on the correlation function and its influence on the results.

The mass dependence of the exact mis-centering fractions (for the brightest galaxy to be the central) are not well understood and mis-centering effects are therefore difficult to model (**??**). We follow the approach outlined in **?** to take the effects of a possible mis-centering of a fraction of the cluster positions into account by modelling the influence on the two-dimensional correlation function.

If a fraction f_{mis} of the galaxy clusters in our sample are mis-centered, then the measured correlation function $\xi'_{\mathrm{2D}}(R)$ is given by

$$\xi'_{\mathrm{2D}}(R) = (1 - f_{\mathrm{mis}})\xi_{\mathrm{2D}}(R) + f_{\mathrm{mis}}\xi_{(\mathrm{2D,mis})}(R), \quad \text{(B1)}$$

where $\xi_{(\mathrm{2D,mis})}$ denotes the contribution of the mis-centered clusters to the correlation function, and $\xi_{\mathrm{2D}}(R)$ corresponds to the contribution of the correctly centered clusters. We model the mis-centered component $\xi_{(\mathrm{2D,mis})}$ as

$$\xi_{(\mathrm{2D,mis})}(R) = \int_0^\infty dR_{\mathrm{mis}} P(R_{\mathrm{mis}})\xi_{(\mathrm{2D,mis})}(R|R_{\mathrm{mis}}), \quad \text{(B2)}$$

where $P(R_{\mathrm{mis}})$ denotes the probability that a cluster is centered at a comoving distance R_{mis} from the brightest galaxy. The contribution $\xi_{(\mathrm{2D,mis})}(R|R_{\mathrm{mis}})$ is related to the correlation function of the correctly centered clusters ξ_{2D} as

$$\xi_{(\mathrm{2D,mis})}(R|R_{\mathrm{mis}}) = \int_0^{2\pi} \frac{d\theta}{2\pi}\xi_{\mathrm{2D}}\left(\sqrt{R^2 + R_{\mathrm{mis}}^2 + 2RR_{\mathrm{mis}}\cos\theta}\right), \quad \text{(B3)}$$

according to **?** and **?**. We model the mis-centering probability $P(R_{\mathrm{mis}})$ as a Rayleigh distribution,

$$P(R_{\mathrm{mis}}) = \frac{R_{\mathrm{mis}}}{\sigma^2}\exp\left(-\frac{R_{\mathrm{mis}}^2}{2\sigma^2}\right), \quad \text{(B4)}$$

Thus, the mis-centered contribution is fully characterized by the two parameters f_{mis} and the witdh of the mis-centering probability distribution σ.

To find the priors for the two mis-centering paramters f_{mis} and σ we cross-match our SZ selected cluster sample with the X-Ray selected ACCEPT cluster sample (**?**). Assuming the ACCEPT clusters to lie at the minimum of the gravitational

Table 4
Listing of the splashback radii inferred by including the effects of
mis-centering of the central cluster positions (labeled with subsricpt 'mis')
as well as the fiducial results for comparison.

gal cat	$R^{2D}_{sp,mis}$	$r^{3D}_{sp,mis}$	R^{2D}_{sp}	r^{3D}_{sp}
PS 21	$1.35^{+0.13}_{-0.12}$	$1.76^{+0.29}_{-0.33}$	$1.384^{+0.088}_{-0.096}$	$1.86^{+0.25}_{-0.26}$
PS 21.5	$1.30^{+0.10}_{-0.10}$	$1.81^{+0.28}_{-0.33}$	$1.323^{+0.080}_{-0.086}$	$1.85^{+0.26}_{-0.30}$
PS 22	$1.33^{+0.13}_{-0.17}$	$1.96^{+0.37}_{-0.45}$	$1.31^{+0.11}_{-0.14}$	$1.90^{+0.32}_{-0.40}$
PS 21.5 (R)	$1.45^{+0.12}_{-0.11}$	$2.23^{+0.27}_{-0.26}$	$1.437^{+0.099}_{-0.089}$	$2.13^{+0.22}_{-0.21}$
PS 21.5 (B)	$1.42^{+0.20}_{-0.25}$	$2.39^{+0.39}_{-0.39}$	$1.43^{+0.12}_{-0.13}$	$2.34^{+0.33}_{-0.34}$

potential, we infer Gaussian priors for the two mis-centering
model parameters $f_{mis} = 0.15 \pm 0.21$ and $\sigma = 0.41 \pm 0.30$.

To study the influence of mis-centering on our findings we
repeat the MCMC model fitting using our new model includ-
ing mis-centering given in Equation **??**, which now includes
two more model parameters.

We find that the use of a projected mis-centering model in-
creases the errorbars on the predicted confidence intervals for
the projected cross-correlation signal by $\sim 25\%$. However, the
effect is barely noticeable in the three-dimensional profiles.
The inclusion of mis-centering is reflected as a small increase
in the inferred errors of the projected and three-dimensional
splashback radii as seen in Table **??**. Although we notice
shifts in the inferred central values of the splashback radii,
none of these shifts appear systematic or significant given the
errors.

C. ESTIMATING THE CONTAMINATION OF THE BLUE GALAXY POPULATION

To infer the color cut which separates star forming (blue)
galaxies from the quenched (red) galaxy population, we cross-
matched the SDSS spectroscopic sample to its Pan-STARRS
photometry. In Figure **??**, we show the plot of the Pan-
STARRS ($g_{P1} - r_{P1}$) color as a function of redshift, and the
color cut we use in our analysis. The SDSS spectroscopic
sample is however quite shallow, and thus consists of galaxies
that are brighter than the Pan-STARRS galaxies that we wish
to cross-correlate. At fainter magnitudes, we can expect red
galaxies to scatter into the blue population due to photomet-
ric errors, potentially contaminating the correlation function
measurement. This could erroneously cause the splashback
feature observed in the blue population. Therefore, we need
to assess the possiblity of such a contamination.

The galaxies that we use in our cross-correlation analysis
for the red/blue galaxy population have an upper absolute
magnitude limit of $M_i - 5 \log h = -18.94$. This corresponds to
a different apparent magnitude limit at each redshift. For each

spectroscopically matched galaxy, we figure out how faint the
apparent magnitude limit in the i_{P1} band is compared to the
actual apparent magnitude of the galaxy, recorded by Pan-
STARRS. Assuming that the populations of galaxies that we
use to cross-correlate with clusters have the same intrinsic col-
ors, but are just fainter, we infer the true intrinsic magnitude
of the galaxies that we cross-correlate in the g_{P1} and the r_{P1}
band. We randomly perturb these magnitudes by the expected
photometric errors at that magnitude.

Next, we compute the fraction of galaxies which were in-
trinsically red that now entered the blue population by the per-
turbation, where we defined the separation of the populations
using the same color cut. We find such a contamination of
intrinsically red galaxies to the blue population to be about
5%. This value would apply for a galaxy population mea-
sured in the field. Given that the red fraction is higher in clus-
ters ($\sim 60\%$ in the whole cluster) than in the field ($\sim 40\%$),
we expect there to be a larger proportion of red galaxies in the
cluster which could potentially contaminate the blue galax-
ies due to photometric errors. This would roughly double the
contamination to be about 10%.

This is a conservative estimate of the contamination, be-
cause the spectroscopic galaxy sample we use has a large in-
completeness at the blue end at redshifts beyond 0.2, where
SDSS targetted the luminous red galaxy population, record-
ing only very few blue galaxies. Thus we are missing a lot
of the blue galaxy population in the highest redshift bins in
our spectroscopic sample. Nevertheless we assess if a $\sim 10\%$
contamination could cause the splashback signal found in the
cross-correlation for the blue galaxies.

The null hypothesis that we would like to establish or rule
out is that the blue galaxies just consist of the infall popu-
lation and show no splashback feature. We assume a sim-
ple $r^{-1.5}$ power law for the 3D cross-correlation of the blue
population consistent for clusters with an infalling popula-
tion, and a 3D cross-correlation equal to the signal found for
the red galaxy population in our analysis. Given these cross-
correlation functions we can estimate the cross-correlation of
the blue population when contaminated with a given amount
of red galaxies, by considering a weighted sum of the two sig-
nals. We find that in order to reproduce the observed cross-
correlation function of the blue galaxies, we need a contami-
nation of about 20%. While our conservatively estimated con-
tamination is smaller than this value, a proper modeling of this
contamination is warranted before definitive conclusions can
be drawn. Larger galaxy surveys with better photometry such
as the HSC or LSST would be of significant help in alleviating
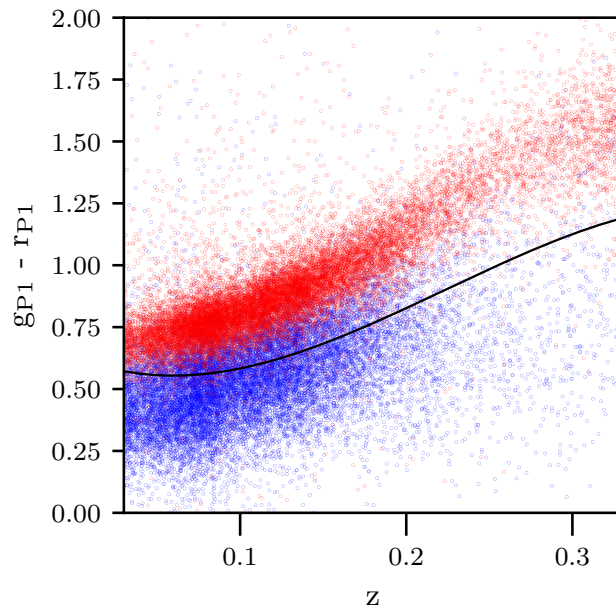these issues.

Figure 7. Scatter plot showing the $(g_{P1} - r_{P1})$ colors of the matched galaxies versus their redshifts, where the red dots correspond to galaxies identified as red from the SDSS spectroscopic colors and blue dots correspond to galaxies identified as blue, respectively. The black, solid line indicates the spline cut separating the two populations and excluding the red galaxies from the blue population at a confidence level of 3σ.